Reaction Kinetics, Mechanisms and Catalysis (2019) 127:449–467
https://doi.org/10.1007/s11144-019-01566-0

Preparation of nano-sized HZSM-5 zeolite with sodium alginate for glycerol aromatization

Ningning Xu[1] · Donghui Pan[1] · Yuanfeng Wu[1] · Siquan Xu[1] · Lijing Gao[1] · Jin Zhang[1] · Guomin Xiao[1]

Received: 3 December 2018 / Accepted: 15 March 2019 / Published online: 1 April 2019

Abstract

A facile method was developed for the synthesis of highly crystallized nano-sized HZSM-5 via adding sodium alginate into zeolite precursor solution. The effects of addition order and dosage of sodium alginate on the physicochemical properties of the catalysts were systematically studied by XRD, FT-IR, TEM, N_2 adsorption–desorption, ICP-OES, ^{27}Al MAS-NMR and NH_3-TPD. It was found that the addition order and dosage of sodium alginate have strong influences on the crystal sizes and acidic properties of the obtained catalysts. About 100 nm crystals were generated in S-HZSM-5-0.75-p through adding the sodium alginate prior to TEOS, which were smaller than the crystal size of conventional HZSM-5 (200–350 nm). However, this method was unfavorable for the incorporation of Al into the framework of HZSM-5. The low content of framework Al could cause a decrease in acidity and the amount of acid sites was only 0.38 mmol g^{-1} in S-HZSM-5-0.75-p, which was slightly lower than conventional HZSM-5 (0.42 mmol g^{-1}). In contrast, smaller crystals (50 nm) and more acid amounts (1.24 mmol g^{-1}) could be obtained for the S-HZSM-5-0.75 synthesized by adding the sodium alginate after TEOS. Nevertheless, the crystals could be easily aggregated to a dandelion-like particles and possessed fewer acid sites when the sodium alginate was added excessively. Under the conditions of 0.1 MPa, 400 °C and a WHSV of 0.96 h^{-1}, a desired 35.06% BTX yield with 8.5 h service lifetime in glycerol aromatization was obtained over S-HZSM-5-0.75 comparing with conventional HZSM-5 (22.19% BTX yield and 3.5 h service lifetime). The remarkable improvement in catalytic performance of nano-sized HZSM-5 zeolite was mainly attributed to the more acid amounts and smaller crystal size, which could increase the accessibility to the acid sites and shorten the diffusion path length.

Electronic supplementary material The online version of this article (https://doi.org/10.1007/s11144-019-01566-0) contains supplementary material, which is available to authorized users.

✉ Guomin Xiao
xiaogm426@gmail.com

[1] School of Chemistry and Chemical Engineering, Southeast University, Nanjing 211189, China

Keywords Nano-sized HZSM-5 · Sodium alginate · Glycerol · Aromatization

Introduction

The widespread increase in the production of biodiesel from plant oils or animal fats has caused the saturation of glycerol market [1]. Glycerol, as a secondary product, is produced via the pyrolysis or fermentation of the biomass cellulose [2]. Unfortunately, the purification of raw glycerol is costly, which is a major obstacle in the chain of biodiesel production. So, if the raw glycerol can be directly utilized and converted to high-added chemicals, then it would be beneficial for the sustainable development of biodiesel.

Benzene, toluene and xylene (BTX), as widely used feedstocks in the chemical industrial process, are mainly derived from petroleum resources [3, 4]. So, efficient conversion of glycerol into aromatic compounds is a viable solution to the shortage of petroleum resources as well as sustainability of biodiesel production. ZSM-5 zeolite exhibits excellent selectivity of BTX in the conversion of glycerol to aromatics (GTA), due to its well-defined microporous structure [2, 4]. However, the sole presence of micropores with pore size below 1 nm seriously restricts the diffusion rates of coke precursors (olefinic and aromatic species). Moreover, these coke precursors could easily polymerize to form coke on acid sites and lead to the deactivation of the zeolite [5, 6].

So far, considerable research efforts have been devoted to overcoming the diffusion limitations caused by micropores, which can be defined as two strategies: one is to introduce mesopores into the zeolite and the other is to minimize the crystal size. In terms of the hierarchical ZSM-5 zeolite, micropores in zeolites possess shape selectivity for the desired products, while the mesopores facilitate the transport of reactants and increase the coke capacity of the catalyst. It is widely accepted that hierarchical ZSM-5 zeolite can be synthesized through the desilication process. The desilication process is closely related to the silicon-aluminum ratio and alkali treatment conditions. Groen et al. [7] provided a comparative study on the effect of atomic ratio Si/Al on the desilication process of ZSM-5 by 0.2 M NaOH solution. It was found that greater mesoporosity could be generated with the generally preserved framework of zeolite in medium Si/Al ratios (25–50). Our previous study [8] synthesized a series of desilicated samples via NaOH solution treatment, and concluded that ZSM-5 zeolite post-treated with mild NaOH solution ($\leq$0.4 M) showed greater improvement in catalytic lifetime in GTA reaction. However, alkali treatment may result in the loss of Al- or Si-containing species, which caused a waste of synthetic raw material and altered acidity properties of zeolites.

With respect to the crystal size of zeolites, it has been reported that nanozeolites structured with small grains (less than 100 nm) can effectively solve the diffusion limitations [9]. Hoang et al. [10] investigated the effects of crystal size of HZSM-5 on the aromatization of propanal and found that smaller crystallites showed slower deactivation. Tang et al. [11] successfully synthesized nanosized ZSM-5 and NaY zeolites inside the mesopore of CNTs. However, this method was very dependent on the mesoporous carbon matrix and not economical. Yang et al. [12] prepared a

series of HZSM-5 zeolites with different size by changing the TPAOH: H_2O ratio and crystallization time and found nano-sized HZSM-5 have remarkable selectivity towards BTX in the methanol to aromatics (MTA) reaction. Nevertheless, the low yield of products restricted this synthesized method on industrial production. Fu et al. [13] proposed a salt-aided seed-induced route to synthesize nano-sized ZSM-5. They found the crystallization process of zeolite was accelerated and the yield of products could reach 85%, but the relative crystallinity was only 45%. Polymers can control the zeolite growth rate and thus affect the crystal size. Wang et al. [14] prepared NaA (20–180 nm) and NaX (10–100 nm) by introducing methylcellulose (MC) hydrogels into zeolite gels. A three-dimensional network of MC was formed via physical bonds at elevated temperature and it can serve as microreactors or nanoreactors for controlling zeolite growth. Wu et al. [15] successfully prepared monodisperse MCM-41 nanospheres with polyvinyl alcohol (PVA). PVA, with a large number of hydroxyl groups, can be adsorbed on the surface of crystals by the strong hydrogen bonding or electrostatic interactions with –Si–OH, thus inhibiting the growth of particles and preventing the agglomeration between particles.

Herein, we introduced a polymer hydrogel, namely, sodium alginate, into the synthesis gel of ZSM-5 and allowed ZSM-5 to crystallize within the three-dimensional network of the crosslinked polymer hydrogel to obtain small crystals. The nano-sized ZSM-5 with high crystalline can be easily synthesized by the addition of sodium alginate. Additionally, the sodium alginate itself is low-cost and non-poisonous. In this paper, the influences of the dosage and adding order of sodium alginate on the catalyst properties and catalytic performances in GTA reaction were discussed in detail. Through this research, we hope to find a new HZSM-5 zeolite with good catalytic performance in GTA reaction.

Experimental

Materials

The reagents including tetrapropylammonium hydroxide (TPAOH, 25 wt % in water), tetraethyl orthosilicate (TEOS, 28.4 wt % SiO_2), aluminum isopropoxide (AIP, 24.7 wt % Al_2O_3), sodium alginate with a kinetic viscosity of 20 cp (1.0 wt % in water) at 20 °C, ammonium chloride (NH_4Cl, 99.5 wt %), methanol (99.5 wt %) and glycerol (99.0 wt %) were purchased from Sinopharm Chemical Reageny Co., Ltd of China and directly used without any further purification. Distilled water was used in all experiments.

Catalyst synthesis

The nano-sized HZSM-5 zeolites were synthesized in a typical procedure. Firstly, 0.56 g AIP was dissolved in 27.5 g TPAOH. Then 25.5 g H_2O was added into the synthesized mixture. After 1 h of stirring, 28.6 g TEOS was added into the synthesis gel and the obtained mixture was stirred at 40 °C for 5 h. Herein, the molar

composition of the synthesized mixture was $100SiO_2$:$1Al_2O_3$:25TPAOH: $2000H_2O$. Subsequently, sodium alginate with different dosage (0.50 g, 0.75 g, 1.00 g, 1.25 g) was added into the precursor solution and the obtained mixture was stirred at 40 °C for 24 h. After that, the prepared mother gel was transferred into a Teflon-lined stainless steel autoclave for further crystallization at 170 °C for 48 h. The obtained catalysts were identified as S-NaZSM-5-x (x = 0.5, 0.75, 1.0, 1.25), where x represented the weight of added sodium alginate. All the samples were calcinated in air at 550 °C for 5 h to remove the organic species. In order to obtain the nano-sized S-HZSM-5-x zeolites, the calcinated zeolites were ion-exchanged three times with 1.0 mol L^{-1} NH_4Cl solution at 80 °C for 8 h, then dried at 80 °C overnight and calcinated at 550 °C for 5 h.

For comparison, the conventional HZSM-5 was synthesized similarly without addition of sodium alginate, and denoted as Con-HZSM-5.

In addition, the influence of the addition order of sodium alginate on the properties of nano-sized HZSM-5 was also investigated. A similar synthesis procedure was performed as follows: first, 0.56 g AIP was dissolved in 27.5 g TPAOH. Then 25.5 g H_2O was added into the synthesized mixture. After 1 h of stirring, 0.75 g sodium alginate was added into the synthesis gel and the obtained mixture was stirred for 1 h. Subsequently, 28.6 g TEOS was added into the precursor solution and the obtained mixture was stirred at 40 °C for 24 h. After that, the prepared mother gel was transferred into a Teflon-lined stainless steel autoclave for further crystallization at 170 °C for 48 h. The obtained catalyst was identified as S-NaZSM-5-0.75-p. All the samples were calcinated in air at 550 °C for 5 h to remove the organic species. In order to obtain the nano-sized S-HZSM-5-0.75-p zeolite, the caclinated zeolite was ion-exchanged three times with 1.0 mol L^{-1} NH_4Cl solution at 80 °C for 8 h, then dried at 80 °C overnight and calcinated at 550 °C for 5 h.

Catalyst characterization

The wide angle (5–50°) powder X-ray diffraction (XRD) patterns were used to identify the phase and evaluate the crystallinity of the catalysts, which was recorded on a Rigaku Ultima IV X-ray diffractometer operating at 40 kV and 20 mA with a Cu K_α radiation source($\lambda = 0.15406$ nm) at a scan step of 20°/min.

Fourier-transform infrared (FT-IR) measurements were performed on a Nicolet 5700 spectrometer and the wavenumber range of the spectra was obtained from 400 to 4000 cm^{-1}.

Transmission electron microscopy (TEM) images were acquired with a FEI Tecnai G2 20 instrument operating at an accelerating voltage of 120 kV.

N_2 adsorption–desorption isotherms were measured to investigate the textural properties of catalysts at − 196 °C using a Beishide 3H-2000 nitrogen absorption instrument. The specific surface areas of all the samples were calculated by the BET method and the microporous volumes were determined by applying the t-plot method. Pore size distribution was obtained from the BJH desorption method.

The temperature-programmed desorption of ammonia (NH_3-TPD) was determined by a Xianquan TP-5076 automated adsorption system with an online thermal

conductivity detector (TCD). Approximately 100 mg of sample was placed in a quartz tube and pretreated at 400 °C for 1 h under flowing He. After cooling to 100 °C, pure NH_3 was introduced to be adsorbed onto the sample for 0.5 h. Then the desorption of NH_3 was accomplished by purging He with a flow of 30 mL/min and rising the temperature to 600 °C at a ramp of 10 °C/min. The desorption profile was determined by TCD.

The Si and Al contents were measured with an inductively coupled plasma optical emission spectrometer (ICP-OES, Varian 720-ES).

Solid-state ^{27}Al MAS-NMR spectra was recorded on an Agilent 600 MHz DD2 spectrometer to detect the distribution of Al in HHZSM-5 zeolite.

Temperature programmed oxidation (TPO) was carried out to measure the carbon deposition of all the spent catalysts on the same TPD apparatus. The deactivated catalyst (100 mg) was first pretreated in He stream at 200 °C for 1 h. After cooling to 50 °C, the TPO profile was obtained by rising the temperature from 50 °C to 800 °C at a ramp rate of 10 °C/min in 5% O_2/He stream.

Catalytic activity measurements

The conversion of glycerol to aromatics was performed in a vertical fixed-bed reactor with an inner diameter of 8 mm at 400 °C and atmospheric pressure. The experimental apparatus for GTA reaction was described in Fig. S1. 1.2 g of the catalyst (40–60 mesh) was packed in the middle of the reaction tube, and then pretreated at 400 °C for 1 h under N_2 flow (30 mL/min) prior to the reaction. The solution of 40 wt % glycerol in methanol was fed by a syringe pump at a WHSV of 0.96 h^{-1} into the reactor through a preheater maintained at a temperature of 295 °C. The products were condensed by a cold tap and analyzed by a GC-7890 gas chromatograph (Shanghai Techcomp Ltd) equipped with a FID detector and a capillary column (SE-30). The internal standard was chlorobenzene. The reactant conversion and product yield were calculated by the following formula:

$$\text{Conversion(C\%)} = \frac{\text{Moles of carbon in converted reactants}}{\text{Moles of carbon in the feed}} \times 100\% \quad (1)$$

$$\text{Product Yield(C\%)} = \frac{\text{Moles of carbon in specific products}}{\text{Moles of carbon in the feed}} \times 100\% \quad (2)$$

In this study, the main focus was liquid products, especially aromatic compounds. Therefore, no detailed gas analysis had been performed. In addition, the conversion of glycerol and methanol was always to 100%. Thus, the carbon yield was approximately equal to the carbon selectivity of specific product.

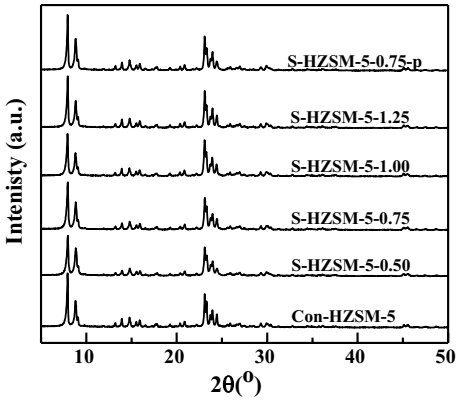

Fig. 1 XRD patterns of the synthesized HZSM-5 samples

Table 1 Crystallinity and lattice parameters of the synthesized HZSM-5 samples

Samples	Crystallization[a] (%)	a/Å	b/Å	c/Å	V/Å^3
Con-HZSM-5	100.0	20.0952	20.0005	14.0444	5644.64
S-HZSM-5-0.50	96.7	20.5781	19.9701	13.5344	5561.92
S-HZSM-5-0.75	103.0	19.6891	20.0332	13.4003	5285.56
S-HZSM-5-1.00	110.1	20.3181	20.0481	12.6778	5164.17
S-HZSM-5-1.25	104.0	19.7611	20.0356	13.4015	5306.00
S-HZSM-5-0.75-p	101.7	19.7637	20.0352	13.4132	5311.22

[a]The relative crystallinity was calculated by the ratio of the diffraction peak area (22.5–25° 2θ) of the sample relative to that of the Con-HZSM-5 as the reference sample (ASTM D5758-01)

Results and discussion

characterization of the samples

The XRD patterns of the synthesized samples are exhibited in Fig. 1. The characteristic diffraction peaks of HZSM-5 appeared in 2θ ranges of 6–10° and 22–25°, suggesting the presence of typical MFI structure inside solid [16, 17]. While no other crystal phase was observed for S-HZSM-5-(x) and S-HZSM-5-0.75-p compared with Con-HZSM-5, which indicated that the synthesized samples were pure HZSM-5 zeolites and crystallized completely [18]. The relative crystallinities of the synthesized samples were calculated according to the method described in ASTM D5758-01 [19] and shown in Table 1. Overall, both for the S-HZSM-5-(x) and S-HZSM-5-0.75-p samples, the relative crystallinities were slightly enhanced, suggesting the crystallization can be promoted with addition of sodium alginate. Obviously, the relative crystallinities of S-HZSM-5-(x) were gradually enhanced and then decreased when the x increased from 0.50 to 1.25. This phenomenon indicated that the proper dosage of sodium alginate could greatly help the crystallization of

HZSM-5 zeolite. The lattice parameters (a, b, c) and cell volumes are also summarized in Table 1. Compared with Con-HZSM-5, a slight deviation of the lattice parameters leading to a decrease in the cell volume was obviously observed in the zeolite modified with sodium alginate. This trend also suggested that the sodium alginate had an influence on the growth of the HZSM-5 zeolite.

To further confirm the framework structures of all synthesized zeolites, the FT-IR characterization was performed (Fig. S2). It can be seen that FT-IR spectra of all the samples were similar with each other. The absorption bands near 450, 550, 800, 1100, 1230 cm^{-1} were the characteristic of HZSM-5 zeolite framework [20, 21], which indicated that all samples possessed typical HZSM-5 framework structures. The result was consistent with the XRD measurements in Fig. 1.

TEM images (Fig. 2) were measured to investigate the morphologies and crystal sizes of all the synthesized zeolites. It was important to point out that the morphology and crystal size distribution were strongly associated with the catalyst property and catalytic performance [22]. The Con-HZSM-5 (Fig. 2a) was rectangular in shape, mainly focusing in range of 200–350 nm. Nevertheless, the TEM images of Figs. 2 and S3 indicated that the particles of S-HZSM-5-(x) samples were mainly composed of nanocrystals (20–60 nm). Apparently, the amount of sodium alginate played a vital role in the morphology of the S-HZSM-5-(x) zeolites. Abundant small nanocrystals (about 50 nm) that accumulated on the large crystals were noted for S-HZSM-5-0.50 in Fig. S3a. However, with the amount of sodium alginate increase, more small nanocrystals (about 50 nm) and fewer large crystals were formed in S-HZSM-5-0.75 (Fig. 2b) and S-HZSM-5-1.00 (Fig. S3b) samples. Interestingly, the small nanocrystals (about 50 nm) would easily agglomerate and aggregate into a dandelion-like particle of about 300 nm for S-HZSM-5-1.25 (Fig. S3c) when the sodium alginate was added excessively. Based on the above results, the guiding role of sodium alginate in the crystal formation process can be speculated. It was well documented in the literature [23] that the -COO- can act as a nucleophile attacking a tetrahedral Si center. Large amounts of hydroxyl and negatively charged carboxyl groups were contained in sodium alginate. Thus, the network structure could be formed by the interaction between sodium alginate (-COO-) and silicon species (-Si–OH). Then zeolite nuclei preferentially generated between the surface of

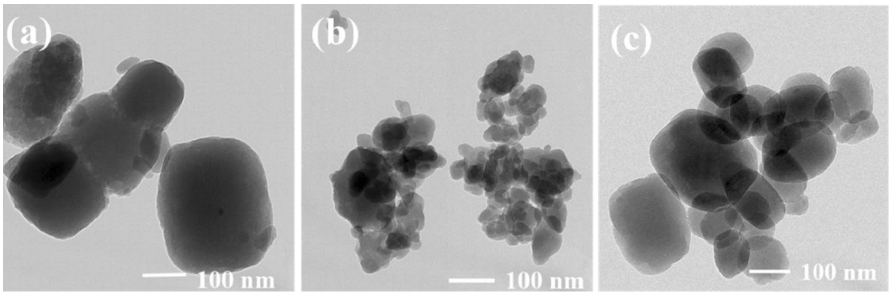

Fig. 2 TEM images of the synthesized HZSM-5 samples: **a** Con-HZSM-5, **b** S-HZSM-5-0.75, **c** S-HZSM-5-0.75-p

sodium alginate and synthesis gel, followed by growing in the network. When the sodium alginate was excessively added, the nano-crystals could be curled up to form secondary particles with dandelion-like nanostructure. This was due to the formation of intermolecular hydrogen bonds between neighbouring sodium alginate [24]. Moreover, the adding order of sodium alginate could significantly affect the crystal size of HZSM-5 zeolites. As demonstrated in Fig. 2c, the crystal size of S-HZSM-5-0.75-p primarily distributed at 100 nm, which was twice larger than S-HZSM-0.75. This was mainly because the carboxyl group of sodium alginate have coordinated with aluminum preferentially [25], leading to an increase in the pore size of the network structure formed by sodium alginate. As a result, the ability of sodium alginate to limit the growth of crystals was weakened. Overall, the modified HZSM-5 with sodium alginate exhibited smaller crystals compared with Con-HZSM-5. And the nano-sized HZSM-5 with about 50 nm crystals could only be synthesized by adding the sodium alginate after TEOS addition. Additionally, obvious aggregation of nanocrystals were also observed in Figs. 2b–c and S3a–c, which might lead to the formation of intercrystal mesopores.

The textural properties of the synthesized samples were characterized by N_2 adsorption–desorption. As shown in Fig. 3, both the isotherms of S-HZSM-5-(x) and S-HZSM-5-0.75-p exhibited a larger hysteresis loop at $P/P_0 = 0.85–1.0$ compared with Con-HZSM-5 zeolite. Such typical characteristic of the intermesopores was mainly generated by the aggregation of nanocrystals [26], which was coincide with the TEM results (Fig. 2).

The detailed textural properties are listed in Table 2. The Con-HZSM-5 possessed relatively low external surface area (168.0 m^2/g) and mesopore volume (0.38 mL/g) while the external surface area and mesopore volume of S-HZSM-5-(x) were up to 202.8 m^2/g and 0.45 mL/g, respectively. The great improvement in textural properties for S-HZSM-5-(x) should be attributed to the generation of nano-sized crystals (50 nm) and more intermesopores. However, the smaller nano-sized particles could be easily aggregated and the excessive aggregation may cause a decrease in external surface and mesopore volume. Especially, the external surface and mesopore volume of S-HZSM-5-1.25 were only 77.3 m^2/g and 0.30 mL/g, which were smaller than

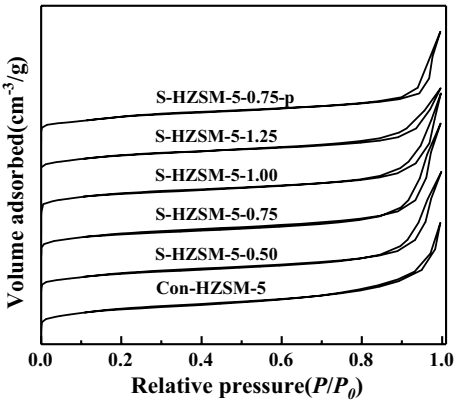

Fig. 3 N_2 adsorption–desorption isotherms of the synthesized HZSM-5 samples

Table 2 Textural properties of the synthesized HZSM-5 samples

Sample	SBETa (m2/g)	Smicrob (m2/g)	Sextb (m2/g)	Vtotal (mL/g)	Vmicrob (mL/g)	Vmesoc (mL/g)
Con-HZSM-5	375.5	207.5	168	0.49	0.11	0.38
S-HZSM-5-0.50	376.7	193.6	183.1	0.53	0.1	0.42
S-HZSM-5-0.75	400	199	200.9	0.57	0.11	0.45
S-HZSM-5-1.00	405.2	202.4	202.8	0.54	0.11	0.41
S-HZSM-5-1.25	391.8	314.5	77.3	0.42	0.16	0.3
S-HZSM-5-0.75-p	390.2	200.8	189.4	0.48	0.1	0.37

[a]From N_2 adsorption measurements (BET method)

[b]From N_2 adsorption measurements (t-plot)

[c]From N_2 adsorption measurements (BJH method)

Con-HZSM-5. From Table 2, it was obvious that the adding order of sodium alginate resulted in some changes in external surface area and mesopore volume. Compared with S-HZSM-5-0.75, smaller external surface area (189.4 m^2/g) and mesopore volume (0.37 mL/g) were observed in S-HZSM-5-0.75-p. This phenomenon was due to smaller crystal size and more intermesopores generated in S-HZSM-5-0.75. Overall, except S-HZSM-5-1.25, S-HZSM-5-(x) samples with increased porosity were expected to exhibit great improvement of the molecules diffusion in GTA reaction.

More importantly, the density of acid sites also plays a key role in catalytic activity and lifetime during GTA reaction. Herein, NH_3-TPD measurements were performed to study acidic properties of the prepared catalysts and the results are presented in Fig. 4. In general, all the samples exhibited two desorption peaks of NH_3, a lower temperature peak (150–300 °C) and a higher temperature peak (350–550 °C), which were assigned to the weak and strong acid sites, respectively [17]. Both the desorption peaks representing strong acid sites for the S-HZSM-5-0.75 and S-HZSM-5-1.00 samples in the TPD curve shifted to higher temperature compared with that of other samples, indicating that the strong acidities in these samples were enhanced [27].

Particularly, the areas of desorption peak were calculated to quantitatively measure the acid amounts of the zeolites and the results are listed in Table 3. It was clearly that the adding dosage of sodium alginate had a profound influence on the density of acid sites for nano-sized HZSM-5. The total acid amount of S-HZSM-5-(x) increased from 0.42 to 1.24 mmol g^{-1}, then decreased to 0.54 mmol g^{-1} when the sodium alginate was added excessively. In addition, when the sodium alginate was added before TEOS, the amount of total acid sites decreased sharply to 0.38 mmol g^{-1}. The amount of acid sites was mainly related to the Al concentration and distribution. The bulk SiO_2/Al_2O_3 ratios of the synthesized catalyst were measured by ICP-OES and shown in Table 3. Compared with Con-HZSM-5, the SiO_2/Al_2O_3 ratios of the catalysts modified with sodium alginate were obvious smaller, indicating higher Al contents were exhibited in the catalysts modified with sodium alginate. Though the SiO_2/Al_2O_3 ratios in the catalysts modified with sodium alginate were similar, the amount of acid sites

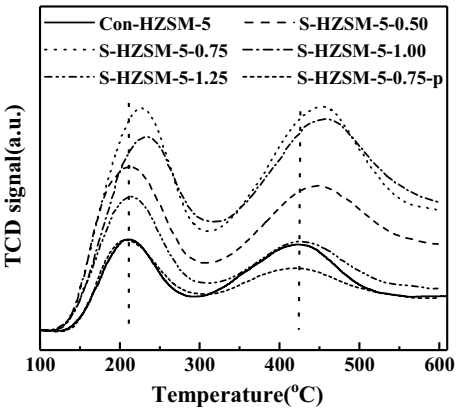

Fig. 4 NH_3-TPD images of the synthesized HZSM-5 samples

Table 3 The distribution of acid amount and SiO_2/Al_2O_3 of the synthesized HZSM-5 samples

Samples	Total acid (mmol NH_3 g^{-1} cat)	Weak acid (mmol NH_3 g^{-1} cat)	Strong acid (mmol NH_3 g^{-1} cat)	SiO2/Al2O3[a] (mol %)
Con-HZSM-5	0.42	0.15	0.27	74.8
S-HZSM-5-0.50	0.86	0.32	0.54	66.4
S-HZSM-5-0.75	1.24	0.44	0.80	50.3
S-HZSM-5-1.00	1.16	0.38	0.78	48.7
S-HZSM-5-1.25	0.54	0.25	0.29	51.2
S-HZSM-5-0.75-p	0.38	0.16	0.22	58.8

[a]Obtained by ICP-OES

varied greatly (Table 3). Jacobsen et al. [28] found the quantification of acidity from NH_3-TPD curves corresponded well with the content of framework Al. That was to say, more extra-framework Al would be generated when the sodium alginate was added excessively or added before TEOS, as obvious decreases of acid amount were observed in S-HZSM-5-1.25 and S-HZSM-5-0.75-p. This should be attributed to that part of aluminum species have coordinated with carboxy groups of sodium alginate rather than bonded with silicon species.

In order to verify the difference in Al distribution of the catalysts, ^{27}Al MAS-NMR spectra (Fig. S4) of Con-HZSM-5, S-HZSM-5-0.75, S-HZSM-5-0.75-p were measured. The spectra displayed two main peaks around 55.6 and 0 ppm, which were assigned to framework tetrahedral Al (FAl^{IV}) and extra-framework octahedral Al ($EFAl^{VI}$) [29]. Compared with Con-HZSM-5, a broad peak centered around 35 ppm was observed in S-HZSM-5-0.75 and S-HZSM-5-0.75-p. This broad peak was assigned to the superposition of distorted pentahedral coordination and distored tetrahedral coordination of Al (DAl) [29, 30]. In addition, a chemical shift of FAl^{IV} band could also be observed for S-HHZSM-5-0.75 and S-HZSM-5-0.75-p. The chemical shift in spectra was related the distribution of framework Al to 12 distinct T-sites of the HZSM-5 structure [31]. Nevertheless, it was infeasible to assign framework Al to various T-sites of the HZSM-5 structures only based on NMR chemical shifts. Thus the FAl^{IV} sitings were not discussed here. The proportions of the three Al species were summarized in Table S3. It can be found that the content of DAl and $FEAl^{VI}$ was significantly improved for S-HZSM-5-0.75-p, which indicated that the extra-framework Al was easier generated over the catalyst prepared with the addition of sodium algimate prior to TEOS. And the obvious decrease in FAl^{IV} content was the main reason for the lowest acid amounts in S-HZSM-5-0.75-p. For S-HZSM-5-0.75, a slight change in the proportion of the three bonds was observed compared with Con-HZSM-5. The increase in DAl content and decrease in FAl^{IV} content made it clear that the sodium alginate could also prevent aluminum species into the framework of zeolite when the sodium alginate was added after TEOS.

Catalytic performance

The catalytic performances of the above prepared catalysts in GTA process were investigated under 0.1 MPa at 400 °C and a WHSV of 0.96 h^{-1} with a fixed-bed reactor. During the reaction time, the conversion rates of glycerol and methanol were close to 100% over all the prepared samples. In this study, the service lifetime of the catalyst was defined as the stage from the start to the time when the obtained BTX yield was less than 10%. From Fig. S5, the main liquid products were aromatics and only trace amount of oxycarbides was detected. The mainly oxycarbides were acrolein, acetone, acetaldehyde and acetol. For aromatics in the liquid product, besides BTX aromatics which were the target product, heavy aromatics including trimethylbenzene, methylethylbenzene, tetramethylbenzene and others were also detected.

The product selectivity for these samples at 2.5 h on stream was investigated and the results are shown in Table 4. The distribution of BTX products was similar on the obtained catalysts, and the most abundant product was xylene, then followed by toluene and benzene. Besides, the selectivity of toluene and xylene was obviously enhanced respectively when the sodium alginate was employed in the sample synthesis, while that of benzene was found without visible change. As listed in Table 4, the higher selectivities of benzene (2.07%) and toluene (13.26%) were achieved over S-HZSM-5-1.00 sample, while 17.94% selectivity of xylene was also found over S-HZSM-5-0.75. There was a difference of the C_9^+ products distribution on the obtained catalysts. The most abundant C_9^+ product for S-HZSM-5-0.50 and S-HZSM-5-0.75 was tetramethyl benzene, while for other catalysts was trimethyl benzene. In addition, the ratios of BTX/aromatics on S-HZSM-5-(x) and S-HZSM-5-0.75-p samples were fewer than Con-HZSM-5 zeolite. Especially for S-HZSM-5-0.50, the ratio of BTX/aromatics was only 75.64%. The phenomenon should be related to the smaller crystal size of S-HZSM-5-(x) and S-HZSM-5-0.75-p samples. As Sikarin Tamiyakul [4] reported that C_9^+ heavy aromatics were the initial aromatic products from the predominant aldol pathway, and these have shorter time to crack to lighter aromatics on smaller crystals. Thus, a higher yield of C_9^+ was observed on S-HZSM-5-(x) and S-HZSM-5-0.75-p and the ratio of BTX/aromatics decreased. Similar results were also gained by Hoang Trung Q [10].

As drawn from Fig. 5, for all the catalysts, the carbon yield of BTX increased at initial stage, then went through a steady period and decreased rapidly with time on stream. Overall, the catalysts modified with sodium alginate exhibited higher BTX yield compared with Con-HZSM-5. The carbon yield of BTX for Con-HZSM-5 was 22.20%, while that for S-HZSM-5-(x) was over 30%. Interestingly, the maximum carbon yield of BTX was observed with 35.06% over S-HZSM-5-0.75 sample. However, adding the sodium alginate prior to TEOS addition could cause a decrease in carbon yield of BTX. For S-HZSM-5-0.75-p, the carbon yield of BTX was only 26.97%. It was important to point out that GTA was a typical reaction catalyzed by acid sites [32]. Sikarin Tamiyakul et al. [4] proposed a reaction pathway for aromatic formation in GTA process: (1) propenal, acetol and acetaldehyde were generated by the dehydration of glycerol; (2) olefin products were generated by the carbonyl bond dissociation of acetaldehyde; (3) heavy aromatics were formed via oligomerization and cyclization of olefin and oxygenates (propenal, propanal,

Table 4 BTX products distribution on the synthesized HZSM-5 samples during GTA process

Catalysts	Selectivity (%)									
	Benzene	Toluene	Xylene	Methyl-ethyl benzene	Trimethyl benzene	Tetramethyl benzene	C_9^+	BTX	Aromatics	BTX/Aromatics
Con-HZSM-5	0.79	6.47	13.69	0.81	1.58	0.11	2.42	20.95	23.37	89.64
S-HZSM-5-0.50	1.16	9.80	17.01	1.94	3.44	3.63	9.01	27.97	36.98	74.82
S-HZSM-5-0.75	1.80	12.82	17.94	1.80	1.54	2.70	6.04	32.56	38.60	84.35
S-HZSM-5-1.00	2.07	13.26	15.49	1.33	1.34	1.32	3.98	30.81	34.79	88.56
S-HZSM-5-1.25	1.64	11.61	16.03	1.04	2.28	1.12	4.44	29.28	33.73	86.81
S-HZSM-5-0.75-p	1.23	9.02	14.22	0.74	3.50	1.07	5.31	24.47	29.78	82.17

reaction condition: 400 °C, atmospheric pressure, collected between 2 and 2.5 h

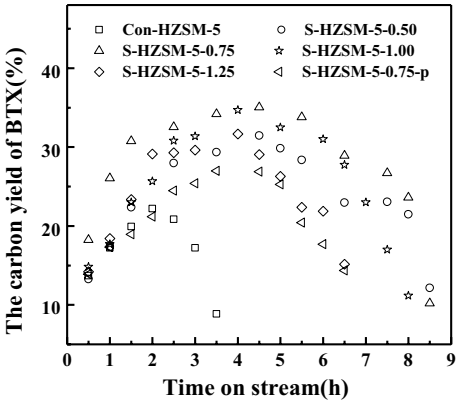

Fig. 5 Time course of the carbon yield of BTX on the synthesized HZSM-5 samples, reaction condition: atmospheric pressure, 400 °C, WHSV = 0.96 h^{-1}

propen-2-ol and methanol); (4) aromatics and short alkanes were generated by the disproportion and cracking of heavy aromatics. Hence, the BTX yield in GTA process was closely related to the acid amounts. Combined with NH_3-TPD (Table 3), the enhanced acid amounts for S-HZSM-5-(x) should be mainly responsible for the improvement of BTX yield. Besides, the improved mass transfer of reactant was also one of important factors for the enhanced catalytic activity [33]. Especially, the carbon yield of BTX for S-HZSM-5-0.75-p was higher than Con-HZSM-5 but the acid sites of S-HZSM-5-0.75-p were the fewest. The improved carbon yield of BTX for S-HZSM-5-0.75-p should mainly be due to the smaller crystal species which made the acid sites more accessible for reactant. As a result, the oligomerization, cyclization and hydrogen transfer steps occurred easily in GTA reaction [34].

The catalytic stability of the catalysts was closely related to the formation of coke. Herein, TPO measurements of the spent catalysts were performed to investigate the formation of carbon deposits and the results are shown in Fig. 6. The TPO spectra of all the prepared catalysts exhibited three combustion peak at 395 °C, 500 °C and 650 °C, which were denoted as coke I, coke II and coke III respectively.

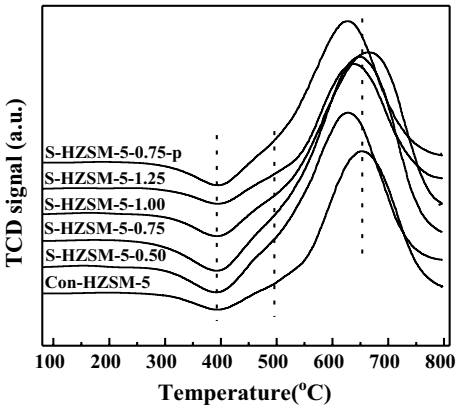

Fig. 6 TPO profiles of the synthesized HZSM-5 samples after GTA reaction

Coke I was assigned to hydrogen-rich carbonaceous deposits, which was mainly formed during aldol condensation procedure [35]. As for coke II, it has more aliphatic nature and was mainly deposited on the external surface, while coke III was mainly polyaromatic carbonaceous deposits [29, 36]. It was obvious that the main coke was polyaromatic carbonaceous deposits (coke III) in GTA reaction. The areas of the three peaks were calculated to quantitatively measure the coke formation rate of the zeolites and the results are listed in Table 5. It was well known that the coke formation rate was strongly influenced by the crystal size, mesoporous volume and acidity [13, 37]. The catalysts modified with sodium alginate had smaller crystal size, which could shorten the diffusion path length and suppress the polymerization of the newly-generated aromatics within micropores. As a consequence, the coke formation rates of S-HZSM-5-(x) and S-HZSM-5-0.75-p were nearly half of the Con-HZSM-5. And the service lifetimes of S-HZSM-5-(x) and S-HZSM-5-0.75-p were obviously prolonged, which were about two times of Con-HZSM-5 (3.5 h). Generally, more acid sites could not only promote the generation of aromatics but also accelerate the formation of coke and the deactivation of catalyst. Although the acid sites of S-HZSM-5-(x) (x = 0.50, 0.75, 1.00) samples were more than S-HZSM-5-1.25, the service lifetimes of the former catalysts (over 8 h) were longer than that of the latter catalyst (6.5 h). The great improvement of service lifetimes on S-HZSM-5-(x) (x = 0.50, 0.75, 1.00) was mainly due to the larger intermesoporous volume, as the intermesopore was favorable to facilitate the diffusion of coke precursors and enhance the accommodation of coke. Overall, both S-HZSM-5-(x) and S-HZSM-5-0.75-p samples could effectively inhibit the carbon deposition in GTA reaction. Comprehensive consideration of BTX yield and service lifetime, S-HZSM-5-0.75 was the most suitable catalyst for GTA reaction.

Regeneration and reusability

To evaluate the reusability of the prepared nano-sized HZSM-5 zeolite, S-HZSM-5-0.75 with the maximum BTX yield was selected as the research object. The spent catalyst was regenerated in air at 550 °C for 5 h and tested in GTA reaction at the same experimental conditions that used previously.

As shown in Fig. 7, the increase in the number of regeneration cycles was accompanied by a gradual decrease in BTX yield. And the BTX yield decreased to 27.48% for the third regenerated catalyst. However, longer service time (up to 11.5 h) on the regenerated catalyst was achieved compared to the fresh catalyst (8.5 h). XRD results in Fig. S6 indicated the structure of the regenerated zeolite was destroyed as the diffraction peak intensity (especially at 22.5–25°) of the catalyst regenerated after three cycles was lower than the fresh catalyst. It was well documented in the literature [36] that the loss of some aluminum from the framework by hydrolysis during the reaction and regeneration should be responsible for the structural damage. Moreover, the loss of aluminum could cause a change in acid properties and textural properties. As shown in Fig. S7 and Table S1, the NH_3-TPD curve areas of the catalyst regenerated after three cycles were much smaller compared with fresh zeolite, and the total acid amount of regenerated catalyst was only 0.29 mmol g^{-1},

Table 5 Amount and nature of the carbon deposits in the synthesized HZSM-5 samples as determined by TPO

Samples	Coke I area (395 °C)	Coke II area (500 °C)	Coke III area (650 °C)	Total area	Service lifetime (h)	Formation rate of carbon deposits (total Area/h)
Con-HZSM-5	585.70	478.87	7589.70	8654.27	3.5	2472.65
S-HZSM-5-0.50	876.70	1280.33	7899.02	10056.05	8.5	1183.06
S-HZSM-5-0.75	1123.90	1170.77	10435.47	12730.15	8.5	1497.66
S-HZSM-5-1.00	706.80	895.78	9762.95	11365.53	8.0	1420.69
S-HZSM-5-1.25	486.60	455.91	6869.65	7812.16	6.5	1201.87
S-HZSM-5-0.75-p	797.90	1152.62	7080.58	9031.10	6.5	1389.40

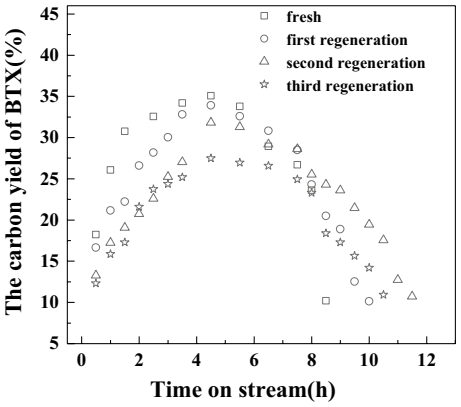

Fig. 7 Time course of the carbon yield of BTX on the regenerated HZSM-5 samples, reaction condition: atmospheric pressure, 400 °C, WHSV = 0.96 h^{-1}

23.4% of the fresh zeolite. The textural properties in Table S2 showed a decrease in the external surface area as well as the mesopore volume of the regenerated catalyst while no change in microporous surface area and microporous volume. Although a catalyst having more acid sites contributed to the formation of aromatic hydrocarbons, it also caused carbon deposition on the surface of the catalyst to occur more easily, and thus the loss of activity was generally faster [38]. Herein, as the regenerated catalyst possessed fewer acid sites, the rate of coke formation was slower, which led to an enhancement in catalytic lifetime.

Conclusions

Highly crystallized nano-sized catalysts were successfully synthesized via the addition of sodium alginate into catalyst synthesis gel. Both the effects of addition order and dosage of sodium alginate on the physicochemical properties and catalytic performance in GTA reaction were studied. The addition of an appropriate amount of sodium alginate after TEOS (S-HZSM-5-0.75) resulted in an obvious decrease in crystal size and increase in external surface area and acid amounts of the zeolite, which could efficiently shorten the diffusion length and improve BTX yield. Nevertheless, the addition of sodium alginate prior to TEOS (S-HZSM-5-0.75-p) led to an unobvious decrease in crystal size and lower acid amounts, which could not significantly promote GTA reaction. As a consequence, 35.06% BTX yield with 8.5 h service lifetime was obtained on S-HZSM-5-0.75 while 26.97% BTX yield with 6.5 h was achieved on S-HZSM-5-0.75-p. This result indicated that the nano-sized HZSM-5 prepared with appropriate amount of sodium alginate after TEOS was a promising catalyst for glycerol aromatization. Although the regenerated S-HZSM-5-0.75 catalyst still had a 27.48% BTX yield in third regeneration cycle, the catalytic activity was significantly decreased compared to the fresh catalyst (35.06% BTX yield). The decreased catalytic activity was mainly due to decrease of acid sites by the loss of aluminum during the reaction and regeneration process. In addition, the service lifetime of the regenerated catalyst was prolonged, which

was up to 11.5 h. This was mainly as the slower carbon deposition rate caused by decreased acid sites, increasing its stability.

Acknowledgements The authors would like to thank the financial support from Fundamental Research for the National Natural Science Foundation of China (No. 21676054, 2140603), Natural Science foundation of Jiangsu (No. BK20161415), Fundamental Research for the Central Universities (No. 2242018K40041).

References

1. Monteiro MR, Kugelmeier CL, Pinheiro RS, Batalha MO, César ADS (2018) Glycerol from biodiesel production: Technological paths for sustainability. Renew Sust Energ Rev 88:109–122
2. Hoang TQ, Zhu XL, Danuthai T, Lobban LL, Resasco DE, Mallinson RG (2010) Conversion of Glycerol to Alkyl-aromatics over Zeolites. Energ Fuel 24:3804–3809
3. Xu XW, Jiang EC, Li ZY, Sun Y (2018) BTX from anisole by hydrodeoxygenation and transalkylation at ambient pressure with zeolite catalysts. Fuel 221:440–446
4. Tamiyakul S, Ubolcharoen W, Tungasmita DN, Jongpatiwut S (2015) Conversion of glycerol to aromatic hydrocarbons over Zn-promoted HZSM-5 catalysts. Catal Today 256:325–335
5. Qi RY, Fu TJ, Wan WL, Li Z (2017) Pore fabrication of nano-ZSM-5 zeolite by internal desilication and its influence on the methanol to hydrocarbon reaction. Fuel Process Technol 155:191–199
6. Yaripour F, Shariatinia Z, Sahebdelfar S, Irandoukht A (2015) Effect of boron incorporation on the structure, products selectivities and lifetime of H-ZSM-5 nanocatalyst designed for application in methanol-to-olefins (MTO) reaction. Micropor Mesopor Mat 203:41–53
7. Groen JC, Jansen JC, Moulijn JA, Pe´rez-Ramı´rez J (2004) Optimal aluminum assisted mesoporosity development in mfi zeolites by desilication. J Phys Chem B 108:13062–13065
8. Xiao WY, Wang F, Xiao GM (2015) Performance of hierarchical HZSM-5 zeolites prepared by NaOH treatments in the aromatization of glycerol. RSC Adv 5:63697–63704
9. Koohsaryan E, Anbia M (2016) Nanosized and hierarchical zeolites: a short review. Chin J Catal 37:447–467
10. Hoang TQ, Zhu X, Lobban LL, Resasco DE, Mallinson RG (2010) Effects of HZSM-5 crystallite size on stability and alkyl-aromatics product distribution from conversion of propanal. Catal Commun 11:977–981
11. Tang K, Wang YG, Song LJ, Duan LH, Zhang XT, Sun ZL (2006) Carbon nanotube templated growth of nano-crystalline ZSM-5 and NaY zeolites. Mater Lett 60:2158–2160
12. Yang LZ, Liu ZY, Liu Z, Peng WY, Liu YQ, Liu CG (2017) Correlation between H-ZSM-5 crystal size and catalytic performance in the methanol-to-aromatics reaction. Chin J Catal 38:683–690
13. Fu TJ, Chang JW, Shao J, Li Z (2017) Fabrication of a nano-sized ZSM-5 zeolite with intercrystalline mesopores for conversion of methanol to gasoline. J Energy Chem 26:139–146
14. Wang HT, Holmberg BA, Yan YS (2003) Synthesis of template-free zeolite nanocrystals by using in situ thermoreversible polymer hydrogels. J Am Chem Soc 125:9928–9929
15. Wu SH, Zhang WW, Jia SY, Liu Y, Ran JY, Ren HT, Hou JW (2013) Novel pathway for the synthesis of monodisperse MCM-41 nanospheres with different particle size distributions. Mater Lett 98:138–141
16. Zhao YH, Gao TY, Wang YJ, Zhou YJ, Huang GQ (2018) Zinc supported on alkaline activated HZSM-5 for aromatization reaction. Reac Kinet Mech Cat 125:1085–1098
17. Tian HF, Zhang ZZ, Chang H, Ma XX (2017) Catalytic performance of imidazole modified HZSM-5 for methanol to aromatics reaction. J Energy Chem 26:574–583
18. Song ZX, Liu W, Chen C, Takahashi A, Fujitani T (2013) Production of propylene from ethanol over ZSM-5 co-modified with zirconium and phosphorus. Reac Kinet Mech Cat 109:221–231
19. ASTM Standard Test Method D5758-01 (2011) Standard Test Method for Determination of Relative Crystallinity of Zeolite ZSM-5 by X-ray Diffraction. West Conshohocken, PA, United States
20. Guo YP, Wang HJ, Guo YJ, Guo LH, Chu LF, Guo CX (2011) Fabrication and characterization of hierarchical ZSM-5 zeolites by using organosilanes as additives. Chem Eng J 166:391–400
21. Majhi S, Dalai AK, Pant KK (2015) Methanol assisted methane conversion for higher hydrocarbon over bifunctional Zn-modified Mo/HZSM-5 catalyst. J Mol Catal A 398:368–375

22. Zhang HB, Ma YC, Song KS, Zhang YH, Tang Y (2013) Nano-crystallite oriented self-assembled ZSM-5 zeolite and its LDPE cracking properties: effects of accessibility and strength of acid sites. J Catal 302:115–125
23. Demadis KD, Mavredaki E, Somara M (2011) Additive-driven dissolution enhancement of colloidal silica. 1. basic principles and relevance to water treatment. Ind Eng Chem Res 50:12587–12595
24. Sabri F, Berthomier K, Marion A, Fradette L, Tavares JR, Virgilio N (2018) Sodium alginate-grafted submicrometer particles display enhanced reversible aggregation/disaggregation properties. Carbohyd Polym 194:61–68
25. Wang H, Fan GL, Zheng C, Xiang X, Li F (2010) Facile sodium alginate assisted assembly of ni-al layered double hydroxide nanostructures. Ind Eng Chem Res 49:2759–2767
26. Tosheva L, Valtchev VP (2005) Nanozeolites: synthesis, crystallization mechanism, and applications. Chem Mater 17:2494–2513
27. Shao J, Fu TJ, Ma Q, Ma Z, Zhang CM, Li Z (2019) Controllable synthesis of nano-ZSM-5 catalysts with large amount and high strength of acid sites for conversion of methanol to hydrocarbons. Micropor Mesopor Mat 273:122–132
28. Jacobsen CJH, Madsen C, Janssens TVW (2000) Zeolites by confined space synthesis-characterization of the acid sites in nanosized ZSM-5 by ammonia desorption and ^{27}Al/^{29}Si-MAS NMR spectroscopy. Micropor Mesopor Mat 39:393–401
29. Ibáñez M, Epelde E, Aguayo AT, Gayubo AG, Bilbao J, Castaño P (2017) Selective dealumination of HZSM-5 zeolite boosts propylene by modifying 1-butene cracking pathway. Appl Catal A 543:1–9
30. Cabral de Menezes SM, Lam YL, Damodaran K, Pruski M (2006) Modification of H-ZSM-5 zeolites with phosphorus. 1. Identification of aluminum species by ^{27}Al solid-state NMR and characterization of their catalytic properties. Micropor Mesopor Mat 95:286–295
31. Biligetu T, Wang Y, Nishitoba T, Otomo R, Park S, Mochizuki H, Kondo JN, Tatsumi T, Yokoi T (2017) Al distribution and catalytic performance of ZSM-5 zeolites synthesized with various alcohols. J Catal 353:1–10
32. Zhang JG, Qian WZ, Kong CY, Wei F (2015) Increasing para-Xylene Selectivity in Making Aromatics from Methanol with a Surface-Modified Zn/P/ZSM-5 Catalyst. ACS Catal 5:2982–2988
33. Tao HX, Yang H, Liu XH, Ren JW, Wang YQ, Lu GZ (2013) Highly stable hierarchical ZSM-5 zeolite with intra- and inter-crystalline porous structures. Chem Eng J 225:686–694
34. Saxena SK, Viswanadham N, Al-Muhtaseb AH (2014) Enhanced production of high octane gasoline blending stock from methanol with improved catalyst life on nano-crystalline ZSM-5 catalyst. J Ind Eng Chem 20:2876–2882
35. Wang F, Zhou MX, Yang XH, Gao LJ, Xiao GM (2017) The effect of hierarchical pore architecture on one-step catalytic aromatization of glycerol: reaction routes and catalytic performances. Mol Catal 432:144–154
36. Wan ZJ, Li GK, Wang CF, Yang H, Zhang DK (2018) Relating coke formation and characteristics to deactivation of ZSM-5 zeolite in methanol to gasoline conversion. Appl Catal A 549:141–151
37. Sun L, Wang XS, Li JC, Ma A (2011) Effect of acidity and diffusibility on coke deactivation over nano-sized HZSM-5 zeolites. Reac Kinet Mech Cat 102:235–247
38. Li JH, Tong K, Xi ZW, Hu ZH, Zhu ZR (2016) Highly-efficient conversion of methanol to p-xylene over shape-selective Mg-Zn-Si-HZSM-5 catalyst with fine modification of pore-opening and acidic properties. Catal Sci Technol 6:4802–4813